



ELSEVIER

Contents lists available at ScienceDirect

NDT&E International

journal homepage: www.elsevier.com/locate/ndteint

Operational and defect parameters concerning the acoustic-laser vibrometry method for FRP-reinforced concrete

Justin G. Chen^a, Robert W. Haupt^b, Oral Buyukozturk^{a,*}

^a Massachusetts Institute of Technology, Department of Civil and Environmental Engineering, 77 Massachusetts Ave., Cambridge, MA 02139, USA

^b MIT Lincoln Laboratory, 244 Wood Street, Lexington, MA 02420, USA

ARTICLE INFO

Article history:

Received 6 July 2014

Received in revised form

15 December 2014

Accepted 17 December 2014

Available online 24 December 2014

Keywords:

Acoustic-laser vibrometry

Non-contact

FRP

Concrete

ABSTRACT

Acoustic-laser vibrometry, a non-contact method for nondestructive testing, was studied by altering operational and defect parameters to determine their effects on measured signatures and system performance. The method detects delamination and voids in fiber-reinforced polymer reinforced concrete by vibrating the material with an acoustic excitation and measuring the vibration signature with a laser vibrometer. The operational parameters studied were excitation sound pressure level, laser signal, angle of incidence, and dwell time. The defect parameters studied were aspect ratio, size, and curvature. This study was undertaken to understand the method's phenomenology and to provide fundamental knowledge for an operational field system.

© 2014 Elsevier Ltd. All rights reserved.

1. Introduction

1.1. Background

Current non-destructive testing (NDT) practices used to detect and locate defects and to quantify material condition in structures typically require measurement devices to be in contact or close proximity with the structure being evaluated. NDT practices of concrete structures include ultrasound, impact echo, and x-ray imaging [1]. In many conditions, the abovementioned methods have been successfully used for decades, however, the proximity requirement can be particularly restricting for bridges, highway overpasses, dams, and others where it may be difficult or dangerous to access the structure to be inspected. This limitation motivates the development of standoff NDT methodologies that can be performed without contact, from a safe operational distance, and that can dramatically increase the inspection area coverage rate.

Popular non-contact NDT methodologies being researched are based on radar, infrared thermography, and laser measurements. Radar is capable of imaging surface and internal defects in concrete structures, however interpretation of the measurement results can be difficult without substantial experience and reference measurements [2]. Infrared thermography uses a camera to image the differential heating or cooling of a concrete structure where air pockets in cement, indicative of a defect, cause thermal

anomalies and is capable of measuring large areas rapidly [3]. A drawback to thermographic imaging is that it provides relatively low resolution and is limited to larger scale defects. Moreover, thermal signals can vary significantly from weather conditions such as solar radiation, atmospheric turbulence, and wind speed. Laser-based methods use an optical beam to measure time varying displacements and particle velocities either through interferometry or vibrometry. In vibrometry, the vibrating surface imparts a modulation onto the optical carrier where the vibration frequency is determined by the Doppler shift and its amplitude by the number of cycle excursions on the carrier. Interferometric methods include holography which images the displacement of an object with a fringe pattern, and shearography which images fringe contours that correlate to the derivative of displacement of the object being measured [4]. Typically these methods are used in conjunction with an induced stress like a flash lamp for heat, so that any abnormalities in the deflections of the object can be measured to determine the presence of a defect. Interferometric data can be difficult to interpret, especially with shearography while holography can be overly sensitive for objects with somewhat large displacements.

A laser vibrometer measures the surface velocity of an object from a distance without physical contact [5]. It does not influence the measurement because no mass is added to the object vibrating, as a contact accelerometer would. They are high resolution because their reference for velocity is the wavelength of light used, which for most systems is on the order of 1 micrometer, allowing for a resolution of a fraction of that wavelength. Also, since the beam size of the laser is small, there is good spatial resolution for the mapping of the surface velocity of an object as long as the

* Corresponding author.

E-mail addresses: ju21743@mit.edu (J.G. Chen), haupt@ll.mit.edu (R.W. Haupt), obuyuk@mit.edu (O. Buyukozturk).

beam can be aimed accurately. The main drawback of the technology is that it is expensive, and scanning systems to map a surface are uncommon and even more expensive.

Laser vibrometers have been used in NDT and sensing applications, with one of the earlier uses being for the detection of defects under fresco paintings [6,7] which has continued to be useful to this day [8]. More recent applications include the testing of brake rotors and engine manifolds in the automotive industry [9], ripeness of fruit [10], land mine detection [11,12], bubbles in paint coatings [13], and damage in composite materials [14–16]. The laser vibrometer has great functionality as a measurement instrument for the NDT of civil infrastructure.

1.2. Concept

A material used in civil infrastructure that lends itself particularly well to measurement by a laser vibrometer is fiber reinforced polymer (FRP) reinforced concrete. This material system consists of FRP, or more colloquially fiberglass, which is bonded with epoxy to concrete for tensile reinforcement, rehabilitation, or environmental protection and its use in civil infrastructure systems has become increasingly popular since the 1990s [18,19]. Defects such as air voids, cracking, delamination, or debonding may occur at the FRP-concrete interface resulting in areas where the FRP is disconnected from the concrete [20]. When externally excited, these areas of disconnected FRP over defects will vibrate differently than intact regions firmly bonded to the concrete, acting like a drum head, vibrating with a specific frequency signature as shown in Fig. 1. The acoustic-laser vibrometry method exploits this phenomenology for the non-contact detection of defects in FRP-reinforced concrete. The acoustic-laser vibrometry system consists of an acoustic excitation source to excite the material being measured, and a laser vibrometer to measure the surface velocity of the material. Analysis of the vibration signal measured in terms of the absolute amplitude or frequency spectrum will determine the presence and approximate size of a defect.

1.3. Objective

Previous work has proven the concept of the acoustic-laser vibrometry methodology for the detection of defects in FRP-reinforced concrete [17,21–23]. Since current testing of the acoustic-laser vibrometry system is conducted under laboratory conditions, it is prudent to study the limits of the performance of the system with regards to varying operational conditions. The objective of this paper is to explore how certain operational parameters affect the performance of the system in terms of the

noise floor, defect vibration velocity, and by extension the signal-to-noise ratio (SNR). The operational parameters studied were the sound pressure level (SPL), laser signal level, angle of incidence, and measurement dwell time. Also different defect configurations with varying aspect ratios, sizes, and surface curvature were measured, and their influence on the measured vibration signatures will be quantified.

The paper will first discuss the experimental materials and methods with an overview of the laboratory acoustic-laser vibrometry system and a description of the test specimens measured. Then an in depth explanation of the theory behind the acoustic-laser vibrometry method, with theoretical explanations for the effects of operational parameters will be given. Defect phenomenology will also be discussed with special attention given to explaining the theory behind the vibration of plates which serves as a model for defects in FRP-reinforced concrete. Results of the measurements will be discussed to explain the effects of the operational and defect parameters on the system performance and the defect response spectrums. Conclusions from the work and suggestions for future developments will be given.

2. Materials and methods

2.1. Experimental setup

The key components of the acoustic-laser vibrometry system are the acoustic source that excites the target and the laser vibrometer that measures the surface velocity of the target as a function of time. A system composed of a commercial laser vibrometer, speaker, and data acquisition equipment was used for experimentation. The laser vibrometer and speaker were positioned carefully to measure the specimen normal to the surface and avoid coupling of the acoustic energy from the speaker directly into the laser vibrometer. Retroreflective tape was used on the target to ensure a good return signal from the target for the laser vibrometer. A simple diagram of the experimental setup is shown in Fig. 2. Basic measurements were made by playing a waveform through the speaker, either a frequency sweep, single tone sine wave, or white noise. The laser vibrometer then measures the velocity time series from the surface of the specimen.

To vary the SPL, the volume on the speaker was increased or decreased, and a microphone was placed in front of the specimen to measure the SPL at the target specimen. The laser signal level was altered by placing neutral density (ND) filters of various transmittances to decrease the amount of light both transmitted and received by the laser vibrometer. For example, an ND2 filter

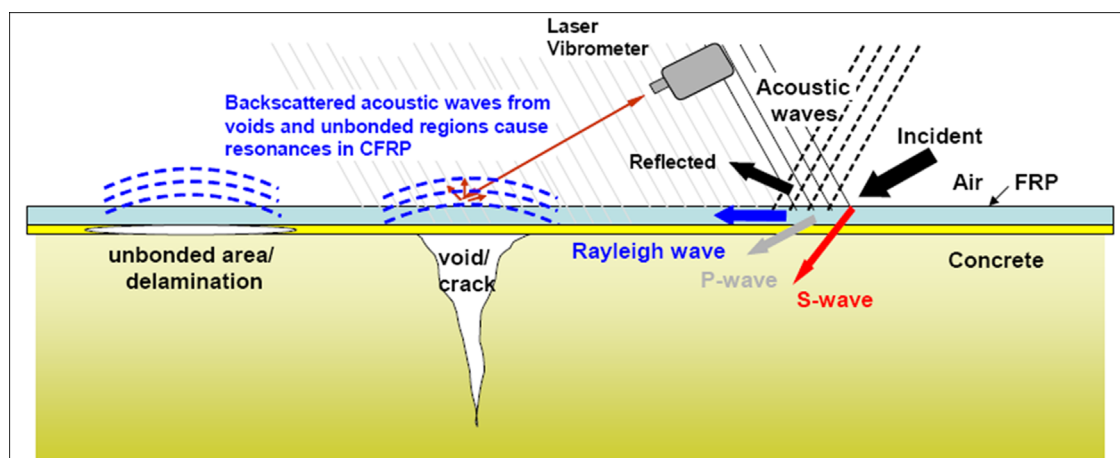


Fig. 1. Acoustic-laser vibrometry [17].

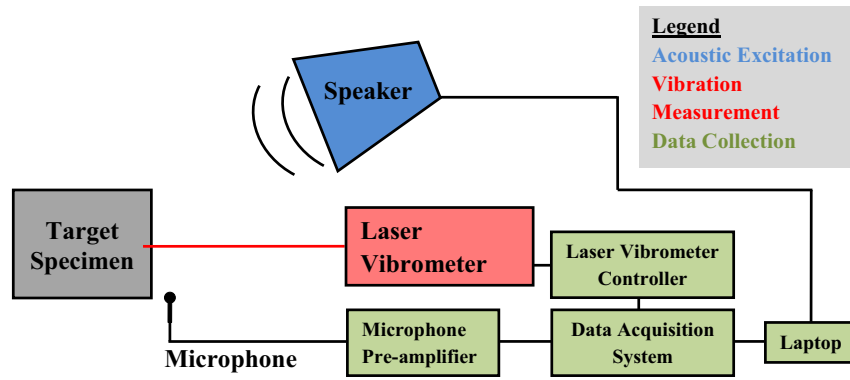


Fig. 2. Diagram of experimental setup.

has a transmittance of 50% and the light received by the laser vibrometer would be 25% of the amount if no filter was used. For the angle of incidence study, the specimen was turned, effectively changing the angle of incidence of both the acoustic excitation and the laser vibrometer. For the measurement dwell time study, shorter segments of data from the same longer data set were processed to determine the effect of a shorter measurement.

2.2. Data processing

The data collected from the laser vibrometer using the data acquisition system is in the form of voltage versus time. Scaling factors were used to obtain the velocity as a function of time for the laser vibrometer or decibels for the microphone. When the specimen was excited by a frequency sweep, the amplitudes were also scaled so that the resultant amplitude would be similar to that of a pure sine wave excitation of a single frequency. This amplitude scaling factor is the square root of the frequency sweep duration multiplied by the frequency bandwidth. The data was processed using a fast Fourier transform (FFT) to transform the data from the time-domain to the frequency-domain to obtain the vibration response frequency spectrum.

2.3. Test specimens

For the system parameter measurements, experimentation was done on the FRPP1 specimen, which has a 3.8 cm × 3.8 cm void defect, shown in Fig. 3a. The specimen is a 30.5 cm × 30.5 cm × 10.2 cm concrete panel with a void to form the defect, on which FRP has been applied using a wet-epoxy layup process. For the angle of incidence test, an additional specimen, FRPS3 was measured, which is an FRP-bonded steel panel with an elliptical defect shown in Fig. 3b.

For the defect parameter tests, several different specimens with different defect configurations were used. For the defect aspect ratio and size test, defects of 7.6 cm in height and varying widths were measured. FRPP2 shown in Fig. 4a has a defect of 7.6 cm × 7.6 cm with a depth of 0.5 cm, and FRPP5 shown in Fig. 4b has defects of height 7.6 cm and depth 2.5 cm, and widths 0.32 cm, 0.64 cm, 1.25 cm, 1.9 cm, and 2.5 cm. The slender defects on FRPP5 are meant to account for defects that may be caused by cracking of concrete rather than delamination. To test the effects of the defect surface curvature when defects occur on round columns, measurements were made on specimens with defects similar to the defects in the FRPP1 and FRPP2 specimens, on concrete cylinders with a diameter of 15.2 cm shown in Fig. 4c and d. FRPC1 has a void defect similar to the FRPP1 specimen that is 3.8 cm × 3.8 cm, and FRPC2 has a delamination-like defect similar to the FRPP2 specimen that is 7.6 cm × 7.6 cm. In general, the test

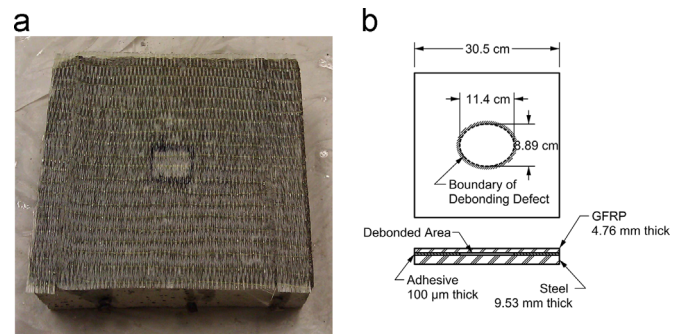


Fig. 3. FRP-bonded test specimens. (a) FRP-bonded reinforced concrete panel, cubic defect, FRPP1 and (b) FRP-bonded steel panel with elliptical defect, FRPS3 [16].

specimen defect sizes are meant to be representative of real defects in FRP-reinforced concrete structures which may experience defects as small as 26 cm² [24].

3. Theory

As previously illustrated in Fig. 1, the general concept behind the acoustic-laser vibrometry system is that air pressure from sound waves will induce vibrations in damaged areas of FRP-reinforced concrete, greater than in surrounding intact areas. The debonding or delamination of FRP allows it to freely vibrate on the surface like a drum head, while in the case of intact material, epoxy firmly bonds the FRP to the concrete. The amplitude of surface vibration is measured with a laser vibrometer that can be aimed to locate the defect with approximately millimeter accuracy. By using a frequency sweep or white noise as the waveform for an acoustic excitation, the specimen is excited over a wide band of frequencies which will include the resonant frequency of the defect. The laser vibrometer measures the surface vibration of the target, obtaining the vibration frequency response to locate and characterize any anomalies. Different defects will have different frequency responses which can be used to estimate the size and shape of a detected defect. In order to describe the theory and phenomenology behind this methodology, three different topics need to be explained. They include the acoustic source exciting the material, defect vibration, and the measurement by the laser vibrometer. The expected effects of altering the operational and defect parameters will be explained.

3.1. Acoustic excitation

The acoustic excitation is what provides energy to vibrate the material so that it can be characterized by the laser vibrometer. The operational parameters that are relevant are the effects of the

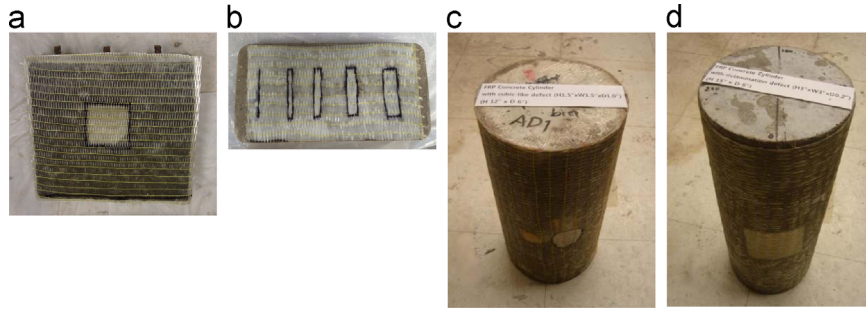


Fig. 4. FRP-bonded concrete panels. (a) FRPP2 and (b) FRPP5 and FRP-confined concrete cylinders, (c) FRPC1 and (d) FRPC2.

sound pressure level (SPL) of the acoustic excitation, and the angle of incidence on the vibration amplitude of the defect. The SPL is a measurement of the air pressure change induced by an acoustic source, related logarithmically to the reference pressure of $20 \mu\text{Pa}$ as given in Eq. (1). An SPL of 80 dB corresponds to a pressure of 0.2 Pa, which is 104 times the reference pressure. In order to relate the SPL to the vibration amplitude we must consider how the air pressure might be related to the velocity of the surface vibration. Sound pressure is directly related to the particle velocity, scaled by an acoustic impedance factor, so we expect that a factor of 10 increase in the sound pressure would also cause a factor of 10 increase in the particle velocity. The factor of 10 increase in the sound pressure, would then mean an increase in the SPL by 20 dB:

$$\text{SPL} = 20 \times \log_{10} \left(\frac{\text{sound pressure in Pascals}}{20 \mu\text{Pa}} \right). \quad (1)$$

For the effect of the angle of incidence on the defect vibration, theoretically there is a simple cosine factor determined by the angle of incidence. The cosine factor scales for the component of the acoustic excitation that is acting perpendicular to the surface, in the direction that the plate is vibrating. With an angle of incidence of 45° the defect should only vibrate $\cos 45^\circ$ or 0.707 times as much as with a normal angle of incidence.

3.2. Defect vibration phenomenology

The parameters to consider when discussing the defect vibration phenomenology are the defect aspect ratio, size, and the surface curvature of the defect. In order to consider these, a mathematical model for the defect must first be formulated. To create a simple model for a delamination, void, or crack defect in FRP-reinforced concrete, only the region of FRP detached from the concrete substrate by the epoxy is considered. The model for the defect is a rectangular or square clamped plate where the resonant frequencies can be determined numerically. Assumptions for this model are that the plate material is isotropic, any void under the plate has a negligible effect on the vibration of the plate, and the boundary where the FRP is bonded to the concrete is assumed to be a clamped condition. The only assumption that does not hold experimentally is that the plate material is isotropic, because FRP is directional, however this should not change too much in the analysis. The numerical values for the defect's resonant frequencies are described by the following equations [25]

$$f = \frac{\lambda}{2\pi a^2} \sqrt{\frac{D}{\rho h}} \quad (2)$$

$$D = \frac{Eh^3}{12(1-\nu^2)} \quad (3)$$

where D is the flexural rigidity of the plate, E is the Young's modulus, h is the thickness of the plate, ν is the Poisson's ratio, ρ is

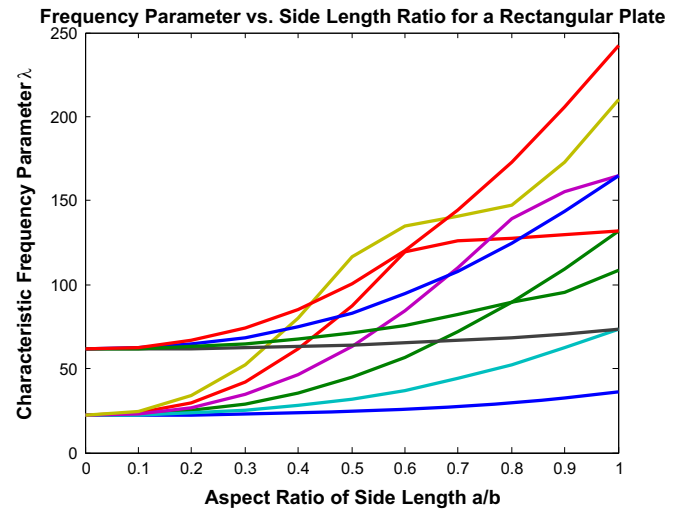


Fig. 5. Plot showing frequency parameter λ as a function of defect aspect ratio [25].

the density of the material, a is the shorter side length of the plate, b is the longer side length of the plate, λ is the frequency parameter that depends on the resonant mode, geometry, and boundary conditions of the plate, and f is the resonant frequency. As a defect gets smaller, the resonant frequencies for the defect increase. For a defect with a curved surface, the effective flexural rigidity of the plate D is increased, and the corresponding resonant frequencies should be higher than if the defect had a flat surface. An example of this increase in stiffness due to curvature is the difference between a piece of paper held flat, which flops down, and a piece of paper held in a curved shape which can support its own weight.

For the effect of the defect aspect ratio, the key parameter here is λ which depends on the boundary conditions, vibrational mode, and a/b the aspect ratio. As the aspect ratio becomes smaller, or as the defect becomes more crack-like and less square, the resonant frequencies corresponding to different vibrational modes shift, as shown in Fig. 5. As the aspect ratio approaches 0, the first seven vibrational modes of a square plate converge to two modes. Therefore, when defects are shaped more like a crack with slender aspect ratios, we expect resonant frequencies to be grouped closer together when the frequencies are normalized to the frequency of the first resonant mode.

4. Results and discussion

A series of parametric studies was conducted to help determine the feasibility of the method and characterize the performance of the laboratory system under different conditions. The parameters that were varied were the incident sound pressure level, laser

signal level, angle of incidence, and measurement dwell time. These parameters can change the noise floor of the system and amplitude measured from the defect, and will alter the detection probability of the system. In order to study the estimated effect of these parameters on the detectability of the sensor system, a receiver operating characteristic (ROC) curve is considered for the acoustic-laser vibrometry system. The ROC curve is a measure of the performance of a binary detector as the true positive rate is plotted versus the false positive rate [26]. The majority of the parametric studies were conducted on the FRPP1 specimen, with Fig. 6a showing a typical measurement. The velocity frequency spectrum is given for defect measurements rather than the more conventional frequency response function (FRF) because in proposed operational usage, the measurement of the acoustic excitation at the actual structure would not be available, and thus an FRF would not be able to be calculated. Fig. 6d shows a ROC curve generated from a grid measurement of the FRPP1 specimen at the first resonant frequency of 3200 Hz [23]. The data was obtained by making a 13 by 10 grid of measurements over an area including the defect and the surrounding intact FRP. The collected data used to generate the ROC curve is shown in Fig. 6c with the image of the defect vibration at 3200 Hz shown in Fig. 6b [23]. To estimate the performance of the system under different parameters, the amplitudes and noise floors of this set of measurements are scaled to give an estimated ROC curve and detectability for the system. The

main simplifying assumption for this estimate is that measurements at the center of the defect to determine the effect of various parameters can be applied to measurements made on other locations on the defect, despite the possibility of a complex vibrational field due to an irregular defect. This assumption is reasonable because the defects are vibrating in the linear range.

4.1. Sound pressure level

The sound pressure level incident on the specimen is a measure of the pressure of the acoustic excitation which causes the response vibration. Effectively this is the strength of the acoustic excitation. A measurement was made varying the SPL from approximately 60 dB to 90 dB as shown in Fig. 7a. The expected relationship where the response velocity increases by a factor of 10 for an increase in SPL of 20, which corresponds to an increase in the actual incident pressure by a factor of 10, was found.

These results can be used to estimate the effect of SPL on the detectability of the system. The SPL is assumed to only influence the vibration amplitude while over the defect and not the noise floor. The scaling factors for the measurements while over the defect are determined from the determined relationship between response velocity and SPL. These scaling factors are used to alter the grid measurements used to generate the ROC curve and an estimate of the ROC curve obtained with higher or lower SPL is

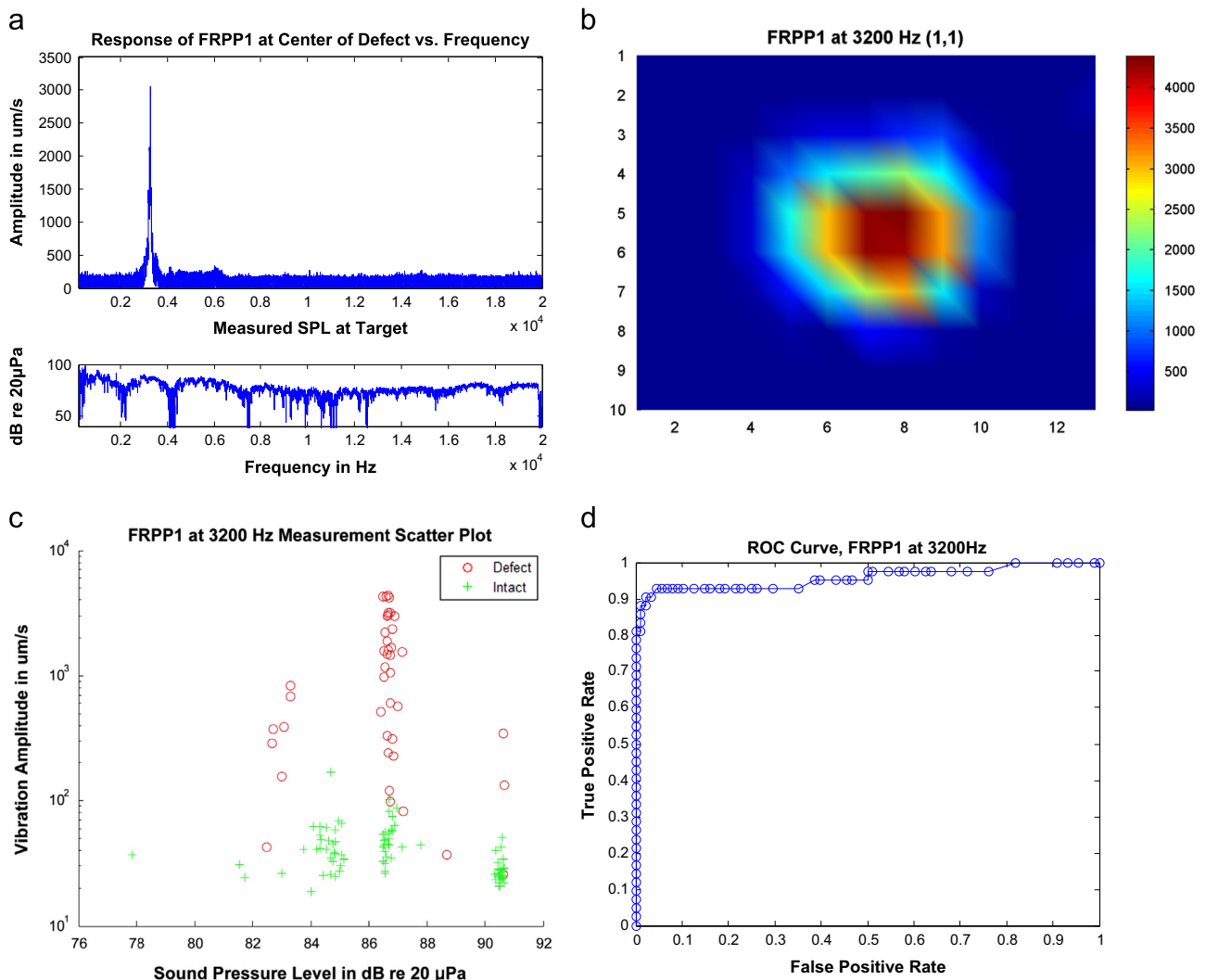


Fig. 6. (a) Measurement at the center of the FRPP1 defect, (b) image of measurement amplitudes of FRPP1 defect at 3200 Hz, (c) plot of measurements of FRPP1 defect at 3200 Hz, and (d) resulting ROC curve [23].

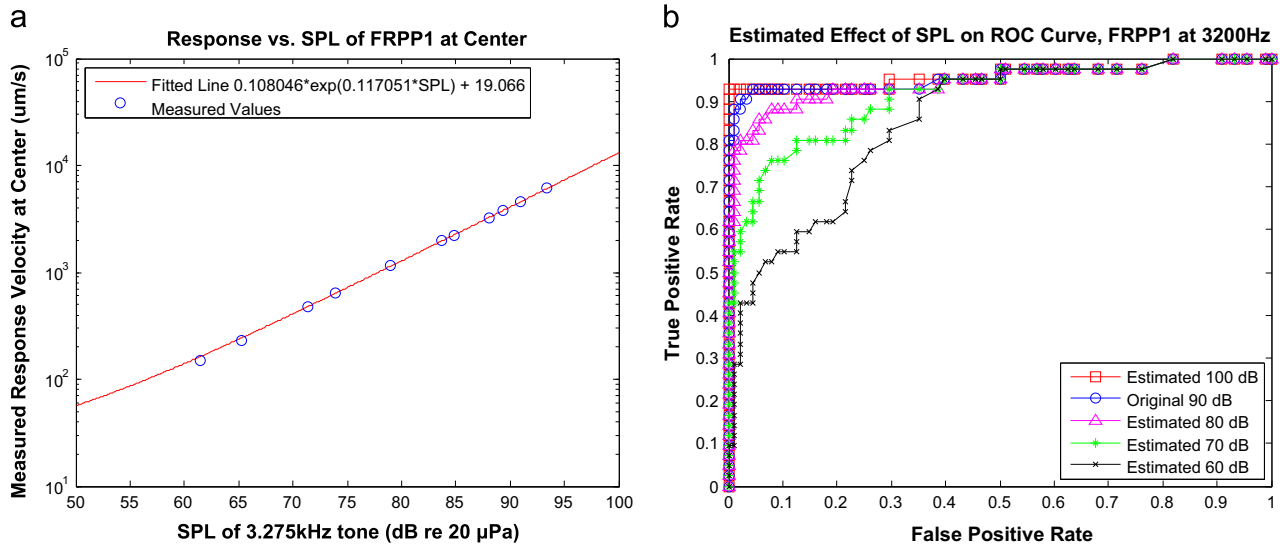


Fig. 7. (a) Response velocity at center of defect versus the incident SPL of the acoustic excitation and (b) estimated effect of SPL on ROC curve for FRPP1 defect at 3200 Hz.

shown below in Fig. 7b. Note that an increase in the sound pressure level over the measurements done at 90 dB has little effect on the detectability of the system.

4.2. SPL distance limitations

The overriding limitation on the distance the system can operate at is likely to be due to the acoustic source, because the SPL at the specimen determines the amplitude of the defect vibration and therefore the amplitude measured by the laser vibrometer. The laser vibrometer range determines the noise floor and can be improved by simply increasing the power of the laser. High power acoustic sources are less common and more difficult to construct and more intrusive to the surrounding environment. From the SPL study, 80 dB is the threshold for an acoustic excitation to sufficiently excite a defect. Since sound intensity follows an inverse square law, SPL decreases by 20 dB for an increase in distance from the acoustic source by a factor of 10. The maximum peak SPL at 1 m from the commercial loudspeaker used is 110 dB and the resulting curve for the SPL of the speaker with distance is shown in Fig. 8. At 32 m the speaker has a peak SPL of 80 dB. Accounting for real world conditions, a more realistic target SPL is 90 dB which results in a maximum distance of 10 m from the commercial loudspeaker.

4.3. Laser signal level

The return laser signal level is an important parameter that will determine the noise floor of the laser vibrometer system. When less power is reflected back from the specimen, either because of poor surface quality, or increase in distance that reduces the amount of light captured by the laser vibrometer lens, the noise floor will increase. Typically, to ensure ideal conditions, retroreflective tape is used on the specimen, which reflects almost all of the incident laser power back to the laser vibrometer lens. However for this measurement, in addition to the use of retroreflective tape, neutral density filters were placed in front of the lens to reduce the amount of laser power both transmitted and received.

From the plot in Fig. 9a, for a factor of 10 reduction in the fraction of light received by the laser vibrometer, the noise floor also increases by a factor of 10. This does not follow the inverse square law theorized for shot noise, and this result may be a characteristic of the signal processing in the commercial laser vibrometer. Since the amount of light reflected back into the laser

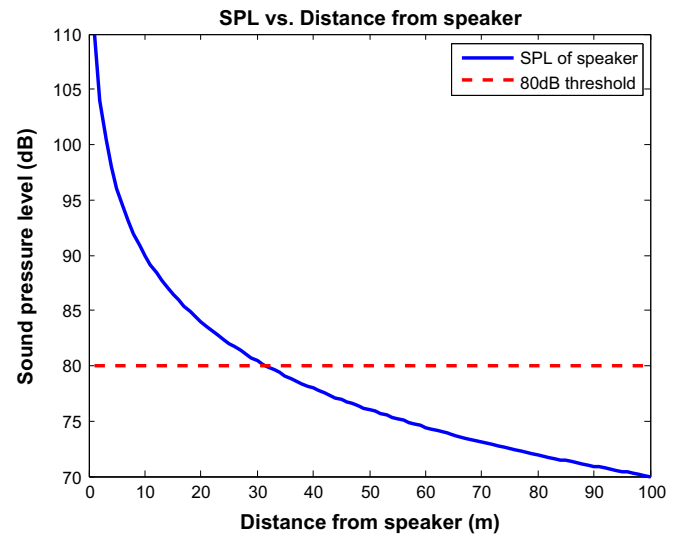


Fig. 8. Sound pressure level vs. distance for commercial loudspeaker.

vibrometer off of a Lambertian surface follows an inverse square law, a factor of 10 reduction in the fraction of light corresponds to a square root of 10 (3.16) increase in distance from the specimen. The effect of lower amounts of transmittance on the ROC curve, which can be scaled to additional distance from the specimen, is shown in Fig. 9b.

4.4. Angle of incidence

The angle of incidence of the measurement system can greatly influence the measured response vibration amplitude. The laser vibrometer only measures movement collinear to the direction of the beam and the amount of power the acoustic excitation imparts to the specimen is greatest at normal incidence; both should follow a cosine dependence as the angle of incidence is changed. Therefore, for this measurement where the angle of the specimen is altered while the position of the laser vibrometer and speaker are fixed, a cosine squared dependence is expected.

In order to make an accurate measurement of the effect of angle of incidence, a different specimen, a prefabricated FRP plate epoxied to a steel plate, designated as "FRPS3", was measured [16]. The surface of the typical FRPP1 specimen was slightly rippled

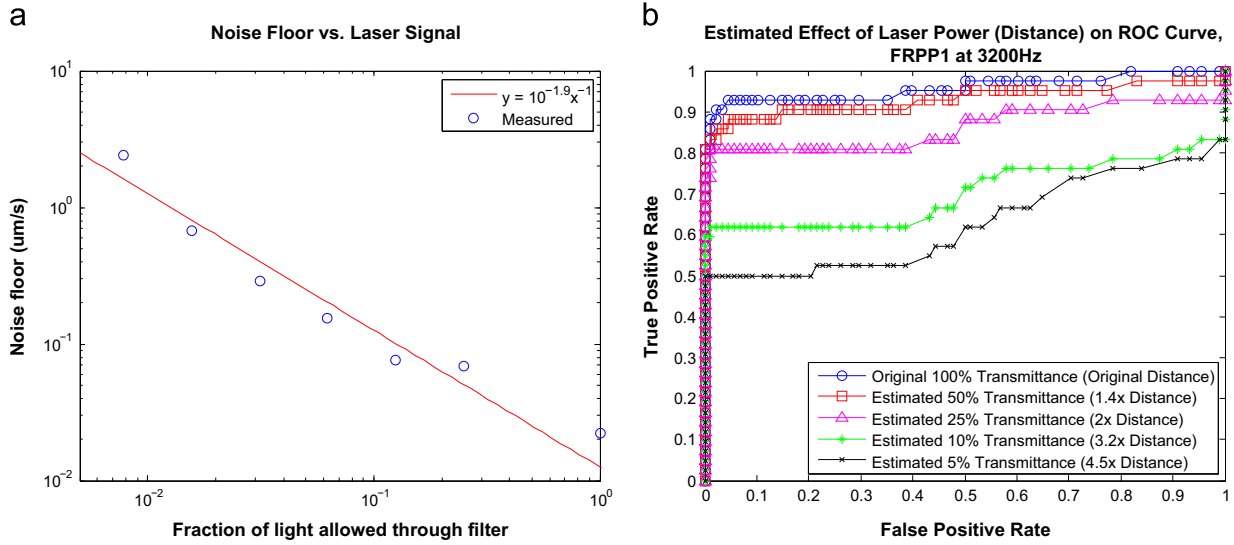


Fig. 9. (a) Noise floor vs. laser signal and (b) estimated effect of laser power (distance) on ROC curve.

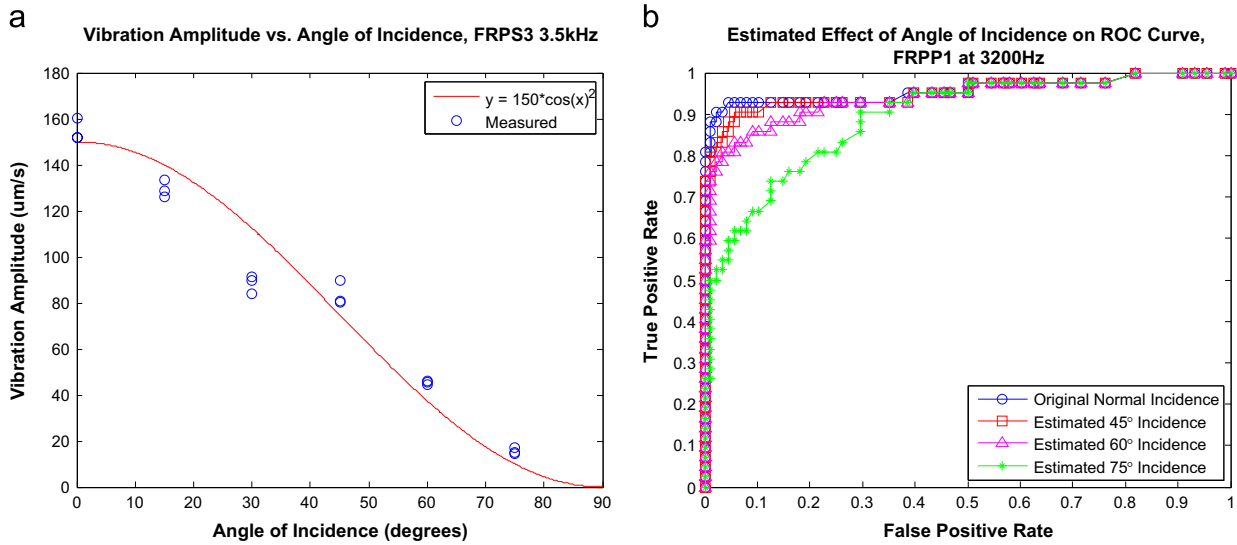


Fig. 10. (a) Vibration amplitude vs. angle of incidence for FRPS3 specimen and (b) estimated effect of angle of incidence on ROC curve for FRPP1 defect at 3200 Hz.

which did not allow for an accurate angle of incidence, and thus the FRPS3 specimen was used. The flatness of the FRP surface allowed for measurement of the vibrational amplitude at angles of incidence: 0°, 15°, 30°, 45°, 60°, and 75°. Fig. 10a shows the plot of the vibration amplitude measurements vs. the angle of incidence with an approximate cosine squared line superimposed over the data. The data followed the expected cosine squared relationship. Fig. 10b shows the estimated effect of different angles of incidence on the detectability of the system. For moderate angles of incidence, such as up to 45°, there is not a large effect on the detectability of the system.

4.5. Measurement dwell time

The measurement dwell time is an important parameter because of the ability to improve the signal-to-noise ratio (SNR) with longer measurements, while a shorter measurement dwell time allows for quicker measurement coverage of an area. Two different acoustic excitations were used to study the effect of dwell time on the measurement. Since the data is fast Fourier transformed, a constant tone sine wave and a white noise waveform will excite the defect differently and change how the vibration

signal peak integrates with time. Plots of SNR and amplitude versus dwell time are shown in Fig. 11a for white noise, and Fig. 11b for a sine wave excitation.

A time of approximately 0.4 ms is necessary to resolve the defect vibration, which corresponds to one cycle of vibration of the defect at the resonant frequency of 3.275 kHz. As dwell time increased, SNR improved at different rates depending on the type of acoustic excitation. For the case of the constant sine wave excitation, when the dwell time increased by a factor of 10,000 from 1 ms to 10 s, the SNR improved by almost the same factor. With the white noise excitation, when the dwell time increased from 1 ms to 1 s, by a factor of 1000, the SNR improved by a factor of only 10, because the amplitude of the vibration decreased. This is a trade off that needs to be made, because a shorter dwell time gives a quicker measurement and the ability to cover more area in a certain amount of time, at the expense of lower detectability.

4.6. Frequency sweep duration

A quick study of varying durations of the frequency sweep and measurement was also performed to determine the change in the SNR if the frequency sweep duration was changed. The

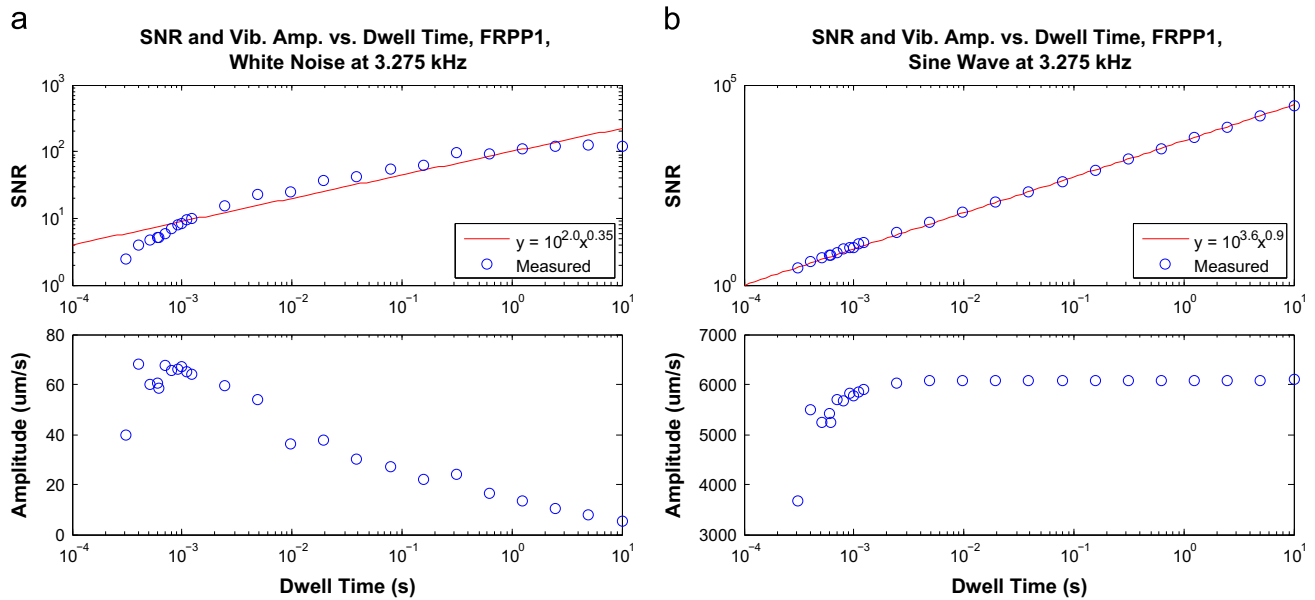


Fig. 11. SNR and vibration amplitude vs. dwell time with (a) white noise and (b) sine wave excitation.

measurements were made with a 0–20 kHz frequency sweep with lengths of 0.1 s, 1 s, 10 s, and 60 s, and other procedures were the same as previous measurements. Table 1 shows the results of the study.

The amplitude and noise floor, and as a result the signal to noise ratio, stays constant despite varying the frequency sweep duration. This suggests that the measurement time can be reduced from 10 s to 0.1 s with no loss in system performance. Also, this suggests that a more complicated processing method for frequency sweep measurements is optimal for extracting the best SNR out of the measurement, for example using a short time Fourier transform (STFT) instead.

4.7. Defect aspect ratio and size

The theory presented dictates that for a square defect, the resonant frequencies should be relatively evenly spaced, and as the defect gets more slender and crack-like, the resonant frequencies should tend to becoming relatively closer together. Plate theory predicts also that a smaller defect should have a higher resonant frequency. In order to study these effects, measurements were made on defects with varying widths of 1.25 cm, 1.9 cm, 2.5 cm, and 7.6 cm, with constant height of 7.6 cm. Fig. 12 shows measurements on the 7.6 cm wide defect FRPP2 at the center and corner. The first resonant frequency in the corner measurement in Fig. 12b is at 1.6 kHz, while the next two resonant frequencies are at 2.25 kHz and 2.8 kHz, for ratios of 1.406 and 1.750. The theoretical ratio for a square clamped plate made of isotropic material should be approximately 2, however FRP is a directional material and is not isotropic, explaining the discrepancy.

Three of the defects of width 2.5 cm, 1.9 cm, and 1.25 cm were measured on the FRPP5 specimen, and the response frequency spectrums are shown in Fig. 13. The narrower crack defects of width 0.32 cm and 0.64 cm when measured did not result in a visible vibrational response from the defect, and are not included. For the 2.5 cm defect shown in Fig. 13a, the first resonant frequency is at 4.15 kHz, the second at 4.5 kHz, and the third at 4.68 kHz. These give ratios of 1.084 and 1.128, which are closer to each other than that of the 7.6 cm defect. For the 1.9 cm defect shown in Fig. 13b, the first resonant frequency is at 6.85 kHz, the second at 7.18 kHz, and the third at 7.54 kHz. The ratios are 1.048 and 1.101. For the 1.25 cm defect shown in Fig. 13c, the first resonant frequency is at 9.45 kHz,

Table 1

Results from frequency sweep duration study.

Sweep length (s)	Frequency (Hz)	Average SPL (dB)	Amplitude ($\mu\text{m/s}$)	Noise Floor ($\mu\text{m/s}$)	SNR
0.1	3247.8	80.3481	5068.0	74.0646	68.4268
1	3245.7	80.4217	4909.4	74.6392	65.7751
10	3246.6	80.4584	4972.1	73.1881	67.9359
60	3247.0	80.2238	5097.8	73.5018	69.3561

the second is at 9.9 kHz, and the third visible is at 11.5 kHz. The ratios are 1.048 and 1.217. One possible reason that the third resonant frequency is comparatively higher, might be that the broad peak of the first and second resonant frequencies hides another resonant frequency of lower amplitude.

Qualitatively, the resonant peaks become broader as the crack width is decreased, and this is seen for all three widths of defect. The reason for this broadening could be that the width of the peaks is relatively large compared to the spacing between peaks, and so they might tend to merge to form one peak instead. The width of the peak is related to the quality factor of the resonance which describes the damping, where the narrower the peak, the lower the damping of the resonance.

Table 2 summarizes the results of the measurements with the resonant frequency, and the ratios of resonant frequencies between the observed first and second and third resonant frequencies, as a function of the defect width. The first resonant frequencies all increase with smaller defect width, confirming the relationship between size of the defect and resonant frequency. The ratio between the second and first resonant frequencies decreases as the defect width decreases, following the prediction from theory. The ratio between the third and first resonant frequencies also decreases for the most part, except for the 1.25 cm wide defect. This confirms that the frequency spacing becomes narrower as defects become more slender.

4.8. Defect curvature

To study the effects of defect curvature, measurements were made on the FRPC1 and FRPC2 column specimens which have defects that are similar to the ones on the FRPP1 and FRPP2 panels. The base frequency of 4.5 kHz of the FRPC1 defect on a column in

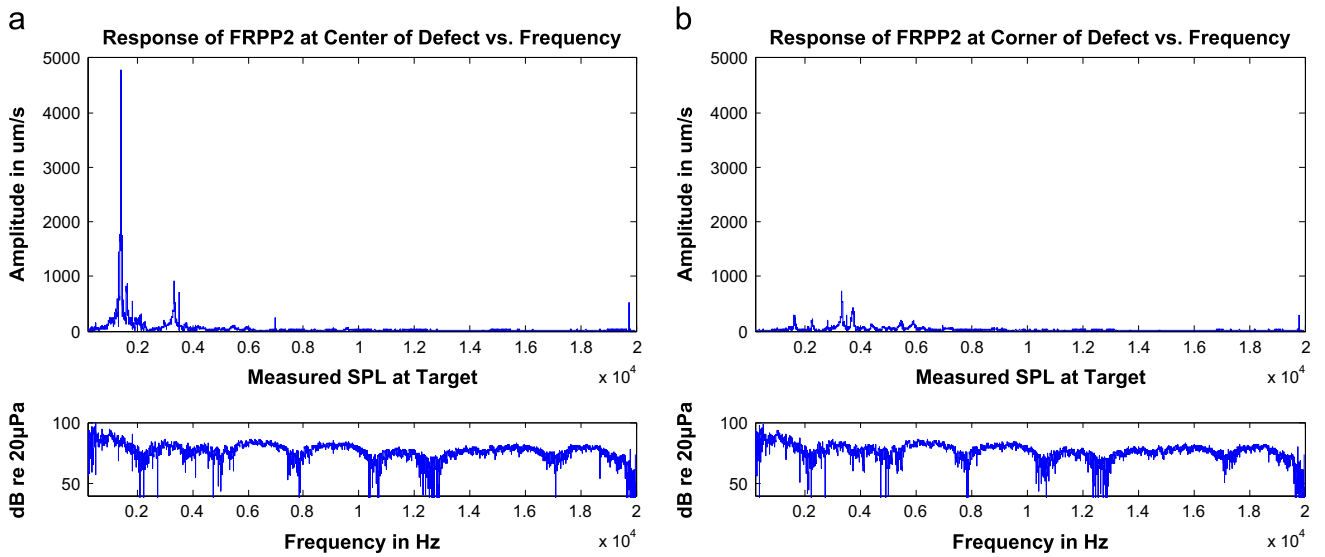


Fig. 12. Frequency response velocity spectrum for FRPP2, 7.6 cm × 7.6 cm defect at the (a) center and (b) corner.

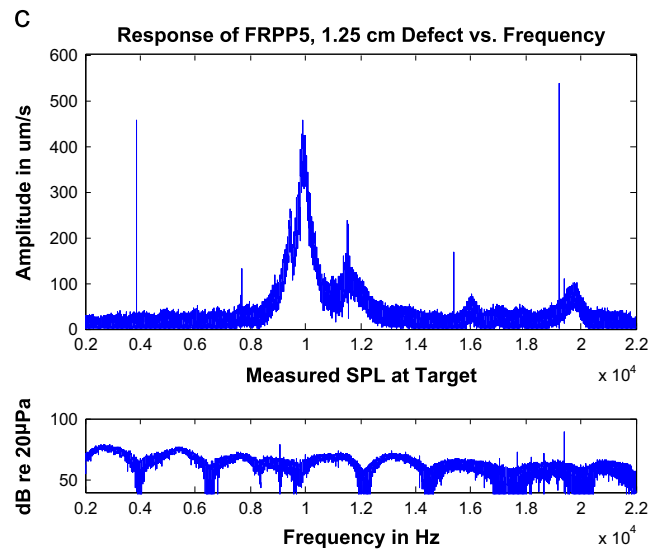
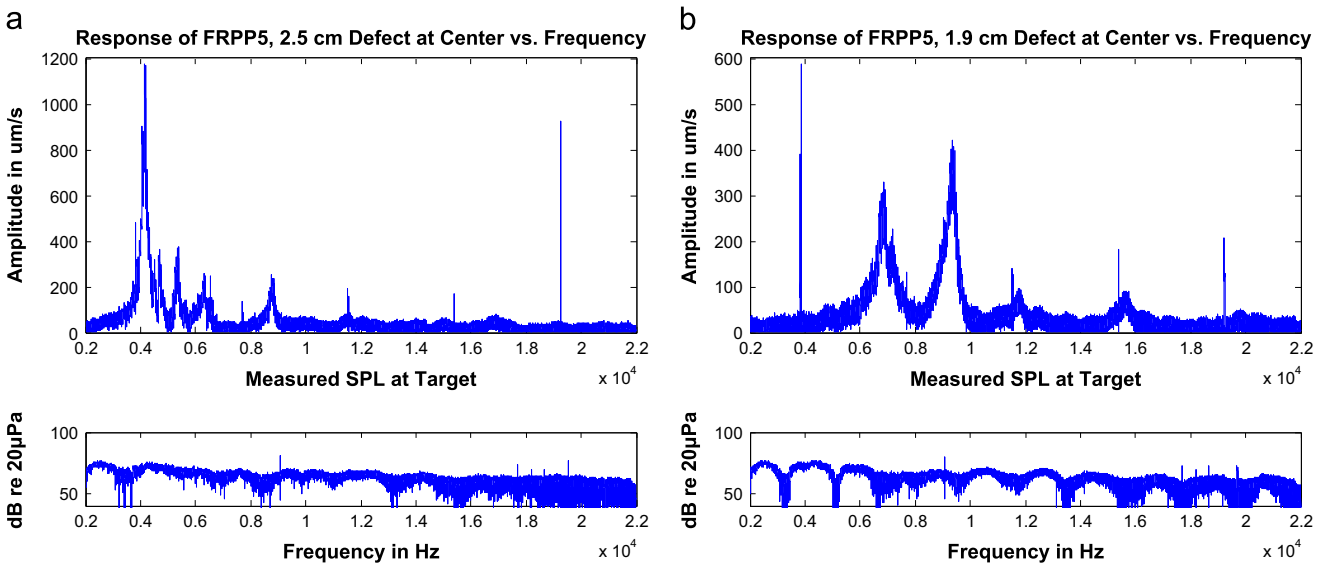


Fig. 13. Frequency response velocity spectrum for FRPP5: (a) 2.5 cm defect, (b) 1.9 cm defect and (c) 1.25 cm defect.

Fig. 14a is greater than the 3.2 kHz of the FRPP1 defect shown previously in Fig. 6a. Similar results are seen in the larger 7.6 cm \times 7.6 cm defects of the FRPC2 specimen shown in Fig. 14b and FRPP2 specimens shown previously in Fig. 12a, with resonant frequencies of 3.2 kHz and 1.6 kHz respectively. This shows that the added stiffness from the curvature of the defect surface increases the resonant frequency of the defect as expected.

5. Conclusion

The measurements of the various specimen configurations in different system configurations provide information about the effects of operational and defect parameters on the performance and signatures measured by the laboratory acoustic-laser vibrometry system. Their effects are summarized as follows. An increase of 20 dB in the sound pressure level at the measured specimen, controlled by the loudness of the acoustic source, will cause a factor of 10 increase in the vibration amplitude, with the effect of increasing the SNR by a factor of 10. An increase in the distance of the laser vibrometer from the target by a factor of two would reduce the laser signal level or amount of light received by the laser vibrometer by a factor of four, thus increasing the noise floor by a factor of four. The acoustic excitation and the laser vibrometer both have a cosine factor due to the angle of incidence. The measurement dwell time for a constant tone sine wave acoustic excitation is directly proportional to the SNR, and for a white noise excitation the cube root of dwell time is proportional to SNR. With a frequency sweep acoustic excitation, for a bandwidth of 0–20 kHz and durations of 0.1–60 s, the SNR is unchanged. The spacing of resonant frequencies of a defect depends on the aspect ratio, where a more slender defect will have smaller relative frequency spacing. As defect size decreases, the first resonant

frequency increases. The addition of defect curvature also increases the resonant frequency due to increased stiffness.

Operationally, measurements for NDT of a structure would involve making closely spaced measurements in a grid to construct an image of the vibration response. Areas with excessive vibration will be indicative of a defect. Since defect sizes are likely to be unknown, the acoustic excitation would need to be broadband, with the frequency sweep being a good candidate, as measurements can be made quickly since 0.1 s measurements provide the same SNR as 60 s measurements. In order to improve the SNR of the measurements, the parameters available to adjust are the SPL and the laser signal level. Angle of incidence is also important, but that will be constrained by system and measurement target positioning in field applications.

5.1. Potential improvements

Improvements in the noise floor of the laser vibrometer will come with increased laser power which increases the amount of light reflected back from the target being measured and received back at the laser vibrometer. The issue is that for field deployment, there is the issue of eye safety as the power of a laser is increased. The commercial laser vibrometer used in this study used a Helium–Neon laser, which is the commonly known red laser at a wavelength of 632.8 nm. If the laser wavelength was instead above 1200 nm the maximum permissible exposure defining the power needed to harm an eye for a given exposure duration, increases by a factor of 10 or more when compared to the visible laser [27]. This would then allow for a more powerful laser that is still eye safe, potentially improving the noise floor and allowing for measurements under adverse conditions. Infrared laser vibrometers are currently available on the market and offer improved performance.

Increases in the strength of the acoustic excitation are another likely source of improvement in the SNR by increasing the amount that the defect is being excited and vibrating. Simply increasing the speaker power is a possible solution, but a more elegant solution involves also using a more focused beam. The parametric acoustic array (PAA) is an acoustic source which uses a high power focused ultrasonic beam to non-linearly generate sound at audible frequencies. In conjunction with the acoustic-laser vibrometry technique, a PAA has been demonstrated to be capable of 100 dB at just under 10 m distance and 80 dB at 100 m distance at a frequency of 1000 Hz, with the source being more powerful for

Table 2
Summary of resonant frequency ratios for different defect widths.

Defect width (cm)	1st freq. (kHz)	Ratio of 2nd/1st freq.	Ratio of 3rd/1st freq.
7.6	1.6	1.406	1.750
2.5	4.15	1.084	1.128
1.9	6.85	1.048	1.101
1.25	9.45	1.048	1.217

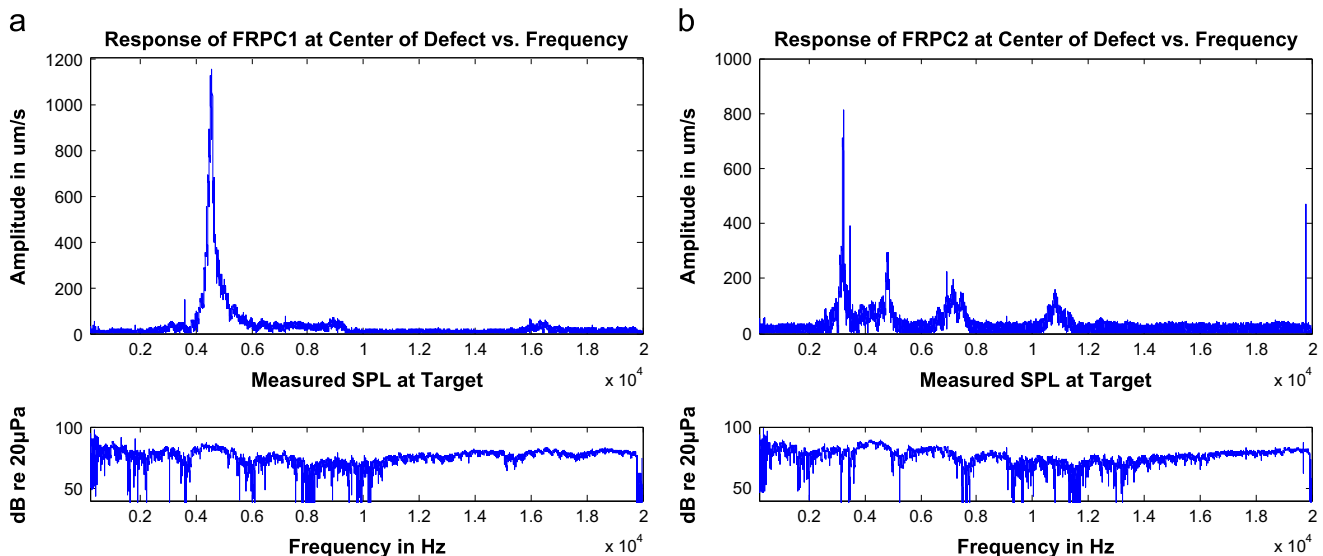


Fig. 14. Measurements of the curved surface defects: (a) 3.8 cm \times 3.8 cm defect on FRPC1 and (b) 7.6 cm \times 7.6 cm defect on FRPC2.

higher frequencies [11]. This would be an improvement over a conventional loudspeaker both because of the increased SPL and the lower amount of acoustic energy wasted as the PAA has a more focused beam.

Acknowledgments

The authors acknowledge the support provided by the National Science Foundation (NSF) under CMMI Grant no. 0926671. The cognizant NSF program managers were Dr. Mahendra Singh and Dr. Kishor Mehta. Special thanks to Tim Emge who assisted with laboratory measurements. MIT Lincoln Laboratory provided the experimental equipment and facilities. At the time of this work, Justin Chen was supported by Royal Dutch Shell through the MIT Energy Initiative. Finally, we express our appreciation of the American Society for Nondestructive Testing (ASNT) for their support through the 2011 Fellowship Award to Professor O. Buyukozturk and graduate student J. Chen.

References

- [1] Büyüköztürk O. Imaging of concrete structures. *NDT & E Int* 1998;31(4):233–43.
- [2] Rhim HC, Büyüköztürk O. Wideband microwave imaging of concrete for nondestructive testing. *J Struct Eng* 2000;126(12):1451–7.
- [3] Lo TY, Choi K. Building defects diagnosis by infrared thermography. *Struct Surv* 2004;22(5):259–63.
- [4] Ganesan A. Holographic and laser speckle methods in non-destructive testing. In: Proceedings of the national seminar and exhibition on non-destructive evaluation, vol. 5; 2009.
- [5] Kachelmyer AL, Schultz KI. Laser vibration sensing. *Linc Lab J* 1995;8(1):3–28.
- [6] Castellini P, Paone N, Tomasini EP. The laser doppler vibrometer as an instrument for nonintrusive diagnostic of works of art: application to fresco paintings. *Opt Lasers Eng* 1996;25(4):227–46.
- [7] Castellini P, Esposito E, Paone N, Tomasini EP. Non-invasive measurements of damage of frescoes paintings and icon by laser scanning vibrometer: experimental results on artificial samples and real works of art. *Measurement* 2000;28(1):33–45.
- [8] Collini L, Garziera R, Mangiavacca F. Development, experimental validation and tuning of a contact-less technique for the health monitoring of antique frescoes. *NDT & E Int* 2011;44(2):152–7.
- [9] Chen F, McKillip D. Measurement and analysis of vibration and deformation using laser metrology for automotive application. *Proc Inst Mech Eng Part D: J Autom Eng* 2007;221(6):725–38.
- [10] Santulli C, Jeronimidis G. Development of a method for nondestructive testing of fruits using scanning laser vibrometry (SLV). *e-J Nondestr Test* 11 (10), 2006.
- [11] Haupt RW, Rolt KD. Standoff acoustic laser technique to locate buried land mines. *Linc Lab J* 2005;15(1):3–22.
- [12] Aranchuk V, Lal A, Sabatier JM, Hess C. Multi-beam laser doppler vibrometer for landmine detection. *Opt Eng* 2006;45(10):104302.
- [13] Beyer S, Gornicki D, Müller G. Analysis of laser-induced vibrations to detect non-adhesive regions of coatings. *Appl Phys A* 2004;79(4–6):1501–4.
- [14] Ghoshal A, Chattopadhyay A, Schulz M, Thornburgh R, Waldron K. Experimental investigation of damage detection in composite material structures using a laser vibrometer and piezoelectric actuators. *J Intell Mater Syst Struct* 2003;14(8):521–37.
- [15] Staszewski W, Lee B, Mallet L, Scarpa F. Structural health monitoring using scanning laser vibrometry. I. Lamb wave sensing. *Smart Mater Struct* 2004;13(2):251.
- [16] Emge T, Buyukozturk O. Remote nondestructive testing of composite-steel interface by acoustic laser vibrometry. *Mater Eval* 2012;70(12):1401–10.
- [17] Buyukozturk O, Haupt R, Tuakta C, Chen J. Remote detection of debonding in FRP-strengthened concrete structures using acoustic-laser technique. In: *Nondestructive testing of materials and structures*. RILEM Bookseries 6, Springer; 2013. p. 19–24.
- [18] Meier U. Strengthening of structures using carbon fibre/epoxy composites. *Construct Build Mater* 1995;9(6):341–51.
- [19] Saadatmanesh H, Ehsani MR. RC beams strengthened with GFRP plates. I. Experimental study. *J Struct Eng* 1991;117(11):3417–33.
- [20] Buyukozturk O, Gunes O, Karaca E. Progress on understanding debonding problems in reinforced concrete and steel members strengthened using FRP composites. *Construct Build Mater* 2004;18(1):9–19.
- [21] Chen JG, Haupt RW, Buyukozturk O. A novel method for the remote detection of debonding in FRP-strengthened concrete: acoustic-laser vibrometry. In: *Proceedings of the ASNT fall conference*; 2012.
- [22] Chen JG, Haupt RW, Buyukozturk O. Remote characterization of defects in FRP strengthened concrete using the acoustic-laser vibrometry method. In: *Proceedings of the ASNT fall conference*; 2013.
- [23] Chen JG, Haupt RW, Buyukozturk O. Acoustic-laser vibrometry technique for the noncontact detection of discontinuities in fiber reinforced polymer-retrofitted concrete. *Mater Eval* 2014;72(10):1305–13.
- [24] Allen DG, Atadero RA. Evaluating the long-term durability of externally bonded FRP via field assessments. *J Compos Construct* 2012;16(6):737–46.
- [25] Leissa AW. *Vibration of plates*. Technical Report. DTIC Document; 1969.
- [26] Fawcett T. An introduction to ROC analysis. *Pattern Recognit Lett* 2006;27(8):861–74.
- [27] International Electrotechnical Commission, *Safety of laser products. Part I. Equipment classification and requirements*, IEC (EN); 2007. p. 60825–1.